Available online at www.eccomasproceedia.org
Eccomas Proceedia COMPDYN (2023) 3559-3569

ECCOMAS
Proceedia

COMPDYN 2023
9th ECCOMAS Thematic Conference on
Computational Methods in Structural Dynamics and Earthquake Engineering
M. Papadrakakis, M. Fragiadakis (eds.)
Athens, Greece, 12-14 June 2023

SELECTION AND SCALING VALIDATION OF GROUND MOTIONS ACCORDING TO TBEC-2018 FOR THE SEISMIC ASSESSMENT OF MASONRY STRUCTURES

Marco F. Funari[1], Shaghayegh Karimzadeh[2], Daniel Caicedo[2], Sayed M. S. Hussaini[2], Aysegul Askan[3], and Paulo B. Lourenço[2]

[1] University of Surrey
School of Sustainability, Civil and Environmental Engineering
Guildford GU2 7XH, UK
m.funari@surrey.ac.uk

[2] University of Minho
Department of Civil Engineering, ISISE, Campus de Azurém 4800-058
Guimarães, Portugal
{ shaghkn, dcaicedod, hussaini, pbl }@civil.uminho.pt

[3] Middle East Technical University
Civil and Earthquake Engineering Departments
Ankara, Turkey
aaskan@metu.edu.tr

Abstract

This paper addresses the selection and scaling of earthquake time histories for analysing masonry structures' Out-Of-Plane (OOP) response according to the 2018 Turkish Building Earthquake Code (TBEC-2018) guidelines. Ground motion simulations are proposed for regions with limited seismic networks or lacking information regarding recorded accelerograms for large-magnitude events. Selection and scaling procedures are automatised according to the TBEC-2018 recommendations. The pre-selection is conducted according to specific seismological characteristics, and the optimal scaling factors of individual records are computed using a metaheuristic optimisation based on the Differential Evolution Method (DEM). Two sets of records (11 real and 11 simulated) are generated and used as input to conduct non-linear dynamic analyses. A U-shaped masonry prototype is adopted as a structural benchmark. The structural response is monitored with an emphasis on the OOP response.

Keywords: Selection and Scaling, Ground motion simulation, Masonry Structures, OOP Response, Metaheuristic optimisation.

ISSN:2623-3347
Peer-review under responsibility of the organizing committee of COMPDYN 2023.
doi: 10.7712/120123.10660.21393

1 INTRODUCTION

Earthquakes have the potential to severely damage historic masonry structures. In order to preserve their structural integrity, advanced numerical models can be utilised to simulate potential ground shaking scenarios and implement appropriate conservation measures. In the last decade, numerical models, either based on the discrete element method or Finite Element Method (FEM), have been extensively used for non-linear dynamic analysis of Historical Masonry Structures (HMS) [1–6]. Discrete element method is particularly suitable for modelling large displacement static or dynamics problems. However, FEM is still the most common approach because of the large spread among practitioners and researchers, despite the limitations of modelling masonry as a homogeneous material [4,7–10]. FEM or DEM are adopted in conjunction with non-linear time history analysis to integrate the equations of motion and determine the structural behaviour. Besides developing a reliable numerical model, the selection of an earthquake input representative of local hazard is a major challenge that might cause uncertainty in assessing the seismic performance of a given structure [11]. In this regard, most relevant seismic codes provide simplified guidelines for scaling and selecting motion records, which have been adopted in past research to evaluate moment-resistant frame structures or bridges [12,13]. However, practitioners tend to use real accelerograms for code-based design validations, which on occasion might be a cumbersome task because of the lack of recorded accelerograms, specifically for the case of large-magnitude events in European regions. To overcome this limitation, simulation techniques have been implemented to reproduce synthetic motions. Ugurhan and Askan [14] performed stochastic simulation based on the dynamic corner frequency approach [15], considering the Duzce (Turkey) Earthquake that took place on November 12th of 1999 (Mw 7.1). Similarly, stochastic simulation has been employed for other historical records, such as the 9th of July 1998 Faial Earthquake (Azores, Portugal) [16].

On the other hand, some authors performed validations on synthetic records. Galasso et al. [17] addressed the validation of hybrid broadband simulation against historical events by considering the response of multiple degrees of freedom systems. Bijelić et al. [18] focused on validation through comparative assessments of building performance using sets of recorded and simulated motions. Similarly, Tsioulou et al. [19] compared the seismic demand of inelastic single-degree-of-freedom systems of hazard-compatible recorded ground motions to the demand of stochastic ground motion modified to match the same target hazard. Furthermore, other investigations adopted simulated records to address engineering and design-related problems. Among them, Karimzadeh et al. [20] performed non-linear time history analyses of multi-story reinforced concrete frames under synthetic records reproduced after the April 6th of 2009 L′Aquila, Italy, earthquake. Recently, the research by Zhong et al. [21] implemented site-specific simulated accelerograms to conduct ASCE 7-16 code-based design checks and performance-based assessment of a 20-story RC moment frame and a 42-story shear wall building.

In this regard, this paper aims to address the seismic assessment of masonry structures by using suites of real and simulated records generated according to TBEC-2018 provisions. The paper is divided as follows. Section 2 presents the derivation of sets of real and simulated motions based on the TBEC-2018 criteria. Section 3 provides a description of the numerical model and FE modelling implementation. The discussion of the results of the non-linear dynamic analyses with a focus on the out-of-plane (OOP) direction is presented in Section 4. Finally, section 5 delivers some relevant conclusions of the study.

2 GROUND MOTION SCALING AND SELECTION

The specific recommendations for selection from TBEC-2018 can be summarised as (i) A minimum of 11 acceleration records should be considered for the analysis; (ii) The spectral

matching should be carried out in the range $0.2T_1$-$1.5T_1$, where T_1 is the fundamental period of the structure; (iii) In the range of matching, the mean spectrum computed from each individual record should be above 1.0 times the code elastic response spectrum for 1- and 2-D analyses or 1.3 for 3-D analyses; (iv) Individual scaling factors lower than 1.3 should be considered. The following subsections describe the process of formulating these guidelines as a constrained optimisation problem and the subsequent selection of both, real and simulated records, to match the target design spectrum.

2.1 Algorithm for selection and scaling

The code-based selection and scaling of groups of acceleration records are handled as a constrained optimisation problem. For this purpose, the Sum of Square Error (SSE) between the mean and target spectral acceleration (*Sa*) spectra is defined as follows:

$$F(x) = \sum_{i=1}^{n} (Sa_{mean}(T_i) - Sa_{ref}(T_i))^2 \tag{1}$$

where *n* is the number of vibration periods considered in the matching domain.

This function is the main objective for minimising to achieve convergence with the target design spectrum. Nonetheless, additional constraints should be taken into consideration to create a global optimisation problem with penalty functions. The first one is referred to as a lower bound for the mean spectrum normally established as 90% with respect to the target spectrum as in [22,23]. An upper bound for the mean spectrum can be defined to construct the generalised first constraint in the form:

$$C_1(x) = \begin{cases} lower\ bound_{mean} - \min\left[{Sa_{mean}(T_i)}/{Sa_{target}(T_i)}\right];\ if\ \min\left[{Sa_{mean}(T_i)}/{Sa_{target}(T_i)}\right] < lower\ bound_{mean} \\ \max\left[{Sa_{mean}(T_i)}/{Sa_{target}(T_i)}\right] - upper\ bound_{mean};\ if\ \max\left[{Sa_{mean}(T_i)}/{Sa_{target}(T_i)}\right] > upper\ bound_{mean} \\ 0;\ otherwise \end{cases} \tag{2}$$

Analogously, a second constraint is defined, this time for lower and upper limits regarding each individual record:

$$C_2(x) = \begin{cases} lower\ bound_{ind} - \min\left[{Sa_{ind}(T_i)}/{Sa_{target}(T_i)}\right];\ if\ \min\left[{Sa_{ind}(T_i)}/{Sa_{target}(T_i)}\right] < lower\ bound_{ind} \\ \max\left[{Sa_{ind}(T_i)}/{Sa_{target}(T_i)}\right] - upper\ bound_{ind};\ if\ \max\left[{Sa_{ind}(T_i)}/{Sa_{target}(T_i)}\right] > upper\ bound_{ind} \\ 0;\ otherwise \end{cases} \tag{3}$$

This constraint was originally proposed in the work of Macedo and Castro [24] to reduce the individual mismatch, so called record-to-record variability. Therefore, the global optimisation problem yields the final form:

$$F(x) = \sum_{i=1}^{n} (Sa_{mean}(T_i) - Sa_{ref}(T_i))^2 + C_1(x) + C_2(x) \tag{4}$$

An additional penalty should be imposed when the same ground motion, or event, is considered more than one in the set. However, a different approach is adopted to decrease the complexity of the objective function. First, a series of seismological conditions (i.e., source mechanism, magnitude, source-to-site distance, and soil conditions) are considered to apply a scenario-based filter to the dataset. Then, the SEE between the acceleration spectrum and the target spectrum is computed, considering the two horizontal components of each record. The filtered set is reorganised by ranking the SEE of each record from lowest to largest in the two directions of analysis, and just the component with the lowest SEE is considered for the next stage. Finally, records from the same event are dropped from the dataset saving only the record of the event with the highest (unscaled) compatibility to the target code spectrum.

Next, a vector **x** is introduced as follows:

$$\boldsymbol{x} = \{x_1, x_2 \cdots x_N\}^T \tag{5}$$

where the value of x_i denotes the i^{th} scaling factor affecting the i^{th} record in a set of N accelerograms, in such a way that the $Sa_{mean}(T)$ vector can be calculated as:

$$Sa_{mean}(T) = \frac{\sum_{i=1}^{N} x_i \, Sa_{ind_i}(T)}{N} \quad (6)$$

where Sa_{ind} is the individual spectra acceleration and N is the number of records, and x_i is the scaling Factor (SF) of the i^{th} record.

The optimisation problem is now aimed at determining the SFs that will reduce the total cost defined earlier in Equation 4. To solve this optimisation problem, the DEM metaheuristic technique is adopted [25].

2.2 Target elastic response spectrum

The city of Istanbul has been selected as location to derive site-specific target spectra considering a standard design earthquake ground motion (10% probability of exceedance in 50 years and return period Tr = 475 years), denoted as earthquake level DD-2 in the TBEC-2018. For the sake of simplicity, the dimensionless spectral acceleration values S_S=0.977 and S_1=0.270 were taken directly from the parameters reported by Işık et al. [26]. These values are utilised for estimating local ground effect coefficients Fs and F_1, the design spectral acceleration coefficients S_{DS} and S_{D1}, and corner periods T_A and T_B. The site-specific design spectrum is computed for a soil class ZC with shear-wave velocity to a depth of 30 meters (V_{s30}) values oscillating in the ranges 360-760 m/s and 180-360 m/s, following the procedure specified in the TBEC-2018.

2.3 Selection of real records

A dataset composed of 1520 three-component recorded accelerograms from various regions in Turkey is considered. For this purpose, two well-known datasets are adopted, including the reference database for seismic ground motion in Europe (RESORCE), [27] and the Turkish Accelerometric Database and Analysis System [28]. The fully integrated dataset consists of 37 earthquake scenarios, with the dominant fault mechanism being strike-slip. Although M_w ranges from 2.8 to 7.6, the most frequent magnitudes are in the range of 4.8-5.2 and 6.4-6.8. The stations are distributed within Joyner and Boore distances (R_{JB}) of up to 744 km and V_{s30} between 131-1862 m/s.

Regarding the selection process, a first scenario-based filter is applied to the complete dataset by fixing some significant seismological parameters (fault mechanism = strike-slip; $M_w \geq 5.5$; fault depth ≤ 40 km; $R_{JB} \geq 15$ km; and V_{s30} in the range 360–760 m/s). The reduced dataset is reorganised according to the SSEs, and the component with less SSE with respect to the target design spectrum is selected. Subsequently, records from the same event with the largest values of SSE are removed from the dataset, and only the first 11 records (best candidates) are taken for the fitting process.

The TBEC-2018 restricts the scaling factors for the modification of real accelerograms to an upper value of 1.3. Nevertheless, and as expected based on the experiences of previous research [29], using SFs lower than 2 led to a poor representation of target spectra. Thus, the searching domain of SFs is fixed in the range of 0.5-5.0. Moreover, the lower and upper bounds for the mean spectrum are set as 1.0 and 1.20 times the target design spectrum, respectively. The spectral mismatch of individual records is limited to ± 50% relative to the target spectrum following Macedo and Castro [24] suggestions. Figure 1 shows the results after scaling 11 real records according to TBEC-2018. Although a good level of matching of the mean spectrum with the target is observed in the relevant domain $0.2T_1$-$1.5T_1$, some values of the mean are below the target spectrum, specifically in the short period range. This behaviour is attributed to

the lack of real accelerograms meeting all the imposed conditions in the scenario-based filtering as well as the limitations of SFs up to 5.0. Similar results were reported in [24] where the implementation of metaheuristic techniques led to suites of records that minimises as better as possible the cost function although not all constraints are fully met in the process.

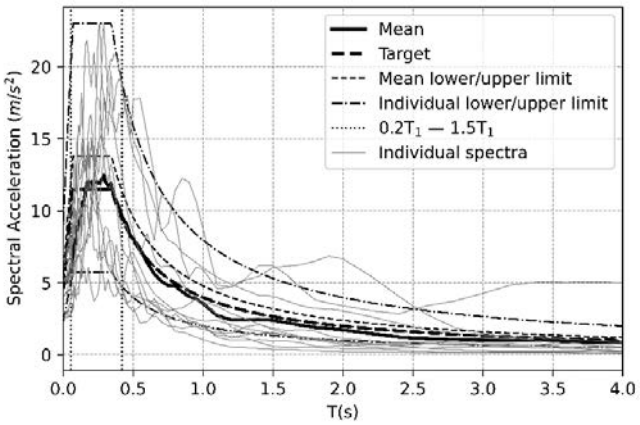

Figure 1. Selection of 11 real records using DE metaheuristic according to TBEC-2018 regulations.

2.4 Selection of simulated records

The dataset of simulated ground motions used in this study consists of 7358 time-series from simulations performed in different regions in Turkey, including Istanbul, Duzce, Van, Afyon, and Erzincan. Among these regions, Duzce, Van, Afyon and Erzincan simulation parameters are validated against previous events [14,30–32] while for Istanbul, the parameters for the hypothetical scenarios are validated against ground motion models [33]. For all regions, three distinct soil types characterised by mean V_{s30} values of 255, 310, and 520 m/s were considered in the simulations. The dataset contains scenarios with M_w ranging from 5.0 to 7.5 and R_{JB} values up to 270 km. For Duzce simulations, the M_w values of the scenario events are 5.0, 5.5, 6.0, 6.5, 7.0, 7.1, and 7.5. For Erzincan simulations, M_w values include 5.0, 5.5, 6.0, 6.5, 7.0, 7.1, and 7.5. For Istanbul, M_w values are 5.0, 5.5, 6.0, 6.5, 7.0, and 7.4, while for Afyon, the M_w range includes 5.0, 5.5, 6.0, 6.5, 6.6, and 7.0. Finally, for the scenario events in Van, the M_w values are 5.0, 5.5, 6.0, 6.5, 7.0, and 7.1.

All of the simulated datasets are constructed using the stochastic finite-fault method as developed by Motazedian and Atkinson [15]. In this approach, the rectangular fault plane is divided into multiple sub-faults, each of which is treated as a stochastic point source. Then, the contribution of each sub-fault is summed up in the time domain with kinematic time delays. This method has been efficiently employed for many regions in the world to simulate the ground motions of large earthquakes.

As with the real records, the preliminary selection is applied to the full simulated ground motion dataset considering the same seismological conditions. The SSEs are also computed, and the records are organised accordingly. However, the selection stage of the earthquake component with a smaller deviation from the target spectrum can be omitted since the simulations are carried out to obtain only a 1-component time-series. Figure 2 depicts the results of the metaheuristic optimisation of the 11 best candidate records to match the target spectrum, considering the same boundaries for the mean spectrum and individual spectra.

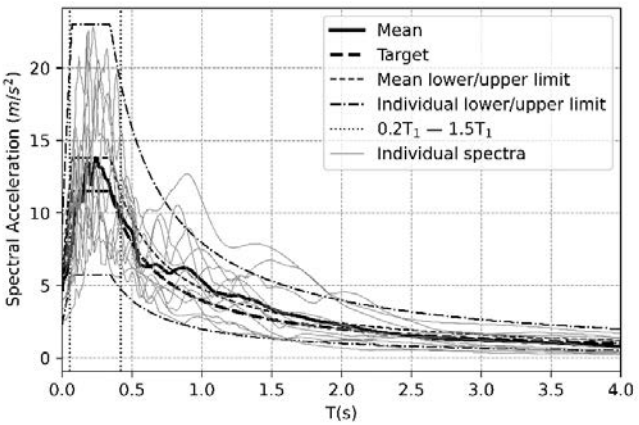

Figure 2. Selection of 11 simulated records using DE metaheuristic according to TBEC-2018 regulations.

For the selection process of simulated records, it was possible to limit the value of SFs up to 2.0, equally achieving an acceptable level of fitting with the target spectrum. These results agree with the discussion presented by Zhong et al. [21] arguing that simulated records reproduce with better accuracy spectral shapes, and therefore, large scaling is not required. Table 1 summarises the selected records alongside their seismological features and SFs. From Table 1 it might be observed that the distribution of SFs is coherent with the distribution of PGA. Real accelerograms exhibit lower values of PGA with higher SFs. An opposite observation is valid for the simulated time-series with higher PGA values; therefore, a better match with the target spectrum is obtained.

Table 1. Seismological characteristics and scaling factors of selected records.

Record Nº	Depth [km]	Comp	Mw	V_{s30} [m/s]	R_{JB} [km]	PGA [m/s^2]	SF
Real records							
1	8.06	N-S	6.8	450	17.86	2.36	2.61
2	15.90	N-S	7.6	701	38.00	2.65	3.48
3	6.09	E-W	5.6	363	15.00	2.46	2.64
4	10.00	S49E	7.0	652	41.00	1.01	4.97
5	14.30	E-W	5.6	481	54.00	1.00	4.97
6	20.00	E-W	6.3	366	52.00	1.32	4.89
7	15.00	E-W	6.0	369	31.00	0.70	5.00
8	10.00	E-W	6.7	433	62.00	0.86	5.00
9	15.00	N-S	6.1	520	43.00	0.53	4.99
10	11.20	N-S	7.1	616	17.00	0.52	4.99
11	5.00	N-S	6.1	529	30.00	0.55	4.98
Simulated records							
1	8.50	—	7.0	520	18.28	3.70	1.74
2	9.50	—	7.0	520	15.90	4.67	1.82
3	7.00	—	6.5	520	18.19	4.92	2.00
4	11.23	—	7.5	520	16.37	3.41	1.87
5	9.50	—	6.6	520	18.19	3.16	1.67
6	8.00	—	6.5	520	15.93	2.08	1.91
7	11.23	—	7.1	520	17.88	2.84	2.00

8	7.00	—	6.0	520	16.21	2.02	1.95
9	6.74	—	7.0	520	17.89	1.69	2.00
10	8.00	—	6.0	520	15.83	2.06	2.00
11	9.55	—	7.0	520	215.98	1.32	1.99

3 PROTOTYPE DESCRIPTION AND FE MODELLING IMPLEMENTATION

A U-shaped masonry prototype is adopted as a structural benchmark in this study. Figure 3 depicts the geometry and overall characteristics of the masonry prototype, which is an abstraction of a single-nave church commonly encountered in earthquake-prone areas of Europe and the Middle East. It is worth noting that these masonry structures have been reported to be among the most damaged typologies in post-earthquake surveys [34].

To account for masonry non-linearities, the Concrete Damage Plasticity (CDP) method, which couples plasticity with a scalar-based damage model [35], is adopted. A linear softening descending branch is used to represent the quasi-brittle nature of masonry in tension. In compression, a plateau is observed after the compressive strength, followed by a linear type of softening. When softening is active, damage variables are introduced to reduce the initial (undamaged) elastic modulus, as expressed by the following equations:

$$\boldsymbol{\sigma_c = (1 - d_c) E_0 (\varepsilon_c - \varepsilon_c^{pl})} \qquad \sigma_t = (1 - d_t) E_0 (\varepsilon_t - \varepsilon_t^{pl}) \tag{7}$$

where E_0 is the elastic modulus of the undamaged masonry, σ_i is the effective stress value; d is the damage parameter relating the effective stress with the corresponding inelastic strain, ε_i is the total strain value, and ε_i^{pl} is the inelastic (plastic) strain value. The subscript i reads as c or t, if associated with the compressive or tensile regime, respectively. A scalar-based damage model describes the damage in tension d_t (cracking) and compression d_c (crushing), which can assume a value between zero (no damage) and one (fully damaged). Under cyclic loading, the masonry structure may experience some loss of stiffness during the unloading phase due to cracking and crushing. To account for non-linear masonry behaviour, the CDP method has been adopted. This method assumes a non-associative flow rule that is represented by a Drucker-Prager hyperbolic function and relies on physically based parameters for accurate modelling. Material properties adopted in the numerical analysis are reported in Table 2.

Table 2. Material properties and model parameters.

E_0[MPa]	ν	ρ [kg m^{-3}]	Dilatation angle	Eccentricity	f_{b0}/f_{c0}	K_c	Viscosity parameter
1000	0.2	1450	10°	0.1	1.16	2/3	0.002

Compressive behaviour			*Tensile behaviour*		
Stress [MPa]	Inelastic strain	d_c	Stress [MPa]	Inelastic strain	d_t
2.20	0	0	0.150	0	0
2.60	0.005	0	0.001	0.003	0.9
0.20	0.012	0.9	0.001	0.010	0.9
0.20	0.020	0.9	-	-	-

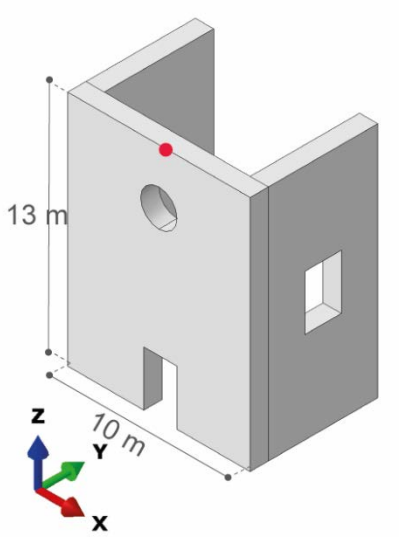

Figure 3. Overall geometry of the U-shaped prototype.

To model damping effects, in this work, the Rayleigh damping model has been adopted. The Rayleigh model approximates the damping coefficient as a linear combination of mass and stiffness, and a damping ratio equal to 3%. The fundamental period of the structure is equal to 0.28 s.

4 RESULTS

This section examines the results of the non-linear dynamic analyses, which have been conducted by using both real and simulated records in the OOP direction of the façade at both polarities. A total of 44 non-linear dynamic analyses are being performed to compare response measures. The results are categorised as “Real” and “Simulated” in Figure 4, which shows their distributions. It is noteworthy that the simulated records provide a more conservative prediction for both base shear and maximum displacement.

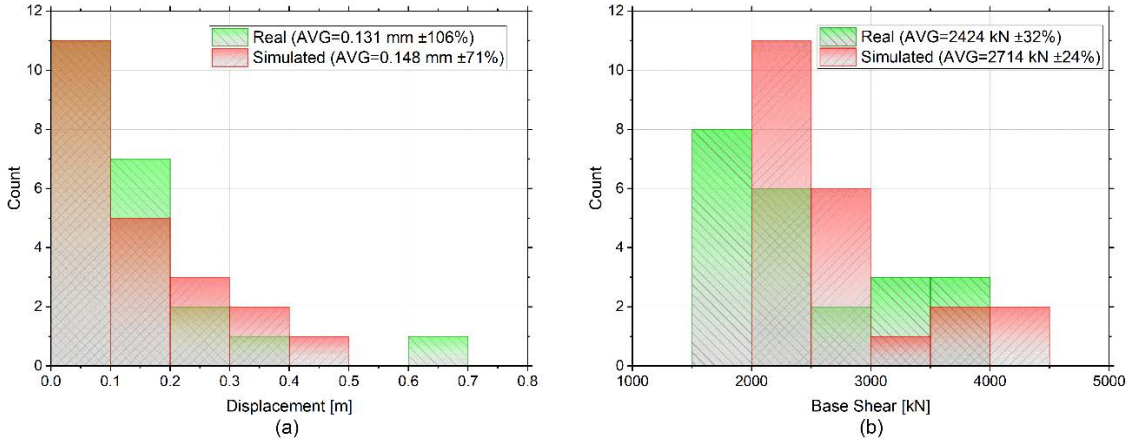

Figure 4. Overall geometry of the U-shape prototype.

5 CONCLUSIONS

This paper addresses the selection and scaling of real and simulated ground motions for the analysis of the OOP response of masonry structures according to the TBEC-2018 provisions. The selection process is formulated as a constrained optimisation problem where the DEM metaheuristic technique is applied to derive the optimal scaling factors of individual records. Two

sets of records (11 real and 11 simulated) matching the DD-2 ZC spectrum in Istanbul city were selected as input to conduct non-linear dynamic analyses for a U-shaped masonry prototype. Simulations are accomplished through the stochastic finite-fault simulation approach based on a dynamic corner frequency concept. The masonry non-linearities were considered by means of the CDP method.

Regarding the selection process, the mean of both sets exhibited close fitting with the target spectrum in the relevant domain $0.2T_1$-$1.5T_1$, although not all constraints were fully met in the optimisation process. In addition, lower SFs were reported for the case of simulated time-series denoting a better match with the target spectrum. The numerical results of the 22 non-linear dynamic analyses conducted for the benchmark structure reveal a clear trend for simulated records to provide a more conservative prediction when analysing shear base and maximum displacement metrics. The findings of this investigation assert that the implementation of a simulated suite of ground motion records exhibits great potential in earthquake engineering applications, particularly with respect to the seismic evaluation of masonry structures.

ACKNOWLEDGMENTS

This work was partly financed by FCT / MCTES through national funds (PIDDAC) under the R&D Unit Institute for Sustainability and Innovation in Structural Engineering (ISISE), under reference UIDB/04029/2020, and under the Associate Laboratory Advanced Production and Intelligent Systems ARISE under reference LA/P/0112/2020. This study has been partly funded by the STAND4HERITAGE project that has received funding from the European Research Council (ERC) under the European Union's Horizon 2020 research and innovation program (Grant agreement No. 833123), as an Advanced Grant. This work is financed by national funds through FCT - Foundation for Science and Technology, under grant agreement UI/BD/153379/2022 attributed to the second author.

REFERENCES

[1] Pulatsu B, Gonen S, Parisi F, Erdogmus E, Tuncay K, Funari MF, et al. Probabilistic approach to assess URM walls with openings using discrete rigid block analysis (D-RBA). Journal of Building Engineering 2022;61:105269. https://doi.org/https://doi.org/10.1016/j.jobe.2022.105269.

[2] Funari MF, Pulatsu B, Szabó S, Lourenço PB. A Solution for the Frictional Resistance in Macro-Block Limit Analysis of Non-periodic Masonry. STRUCTURES 2022.

[3] D'altri AM, Sarhosis V, Milani G, Rots J, Cattari S, Lagomarsino S, et al. Modeling Strategies for the Computational Analysis of Unreinforced Masonry Structures: Review and Classification 2020;27:1153–85. https://doi.org/10.1007/s11831-019-09351-x.

[4] Sarhosis V, Lemos J V, Bagi K. Chapter 13 - Discrete element modeling. In: Ghiassi B, Milani GBT-NM of M and HS, editors. Woodhead Publishing Series in Civil and Structural Engineering, Woodhead Publishing; 2019, p. 469–501. https://doi.org/https://doi.org/10.1016/B978-0-08-102439-3.00013-0.

[5] Funari MF, Spadea S, Lonetti P, Fabbrocino F, Luciano R. Visual programming for structural assessment of out-of-plane mechanisms in historic masonry structures. Journal of Building Engineering 2020;31. https://doi.org/10.1016/j.jobe.2020.101425.

[6] Guo Y, Nagy AP, Gürdal Z. A layerwise theory for laminated composites in the framework of isogeometric analysis. Compos Struct 2014;107:447–57. https://doi.org/10.1016/j.compstruct.2013.08.016.

[7] Bertolesi E, Silva LC, Milani G. Validation of a two-step simplified compatible homogenisation approach extended to out-plane loaded masonries. International Journal of Masonry Research and Innovation 2019;4:265. https://doi.org/10.1504/IJMRI.2019.10019407.

[8] Funari MF, Silva LC, Mousavian E, Lourenço PB. Real-time Structural Stability of Domes through Limit Analysis: Application to St. Peter's Dome. Https://DoiOrg/101080/1558305820211992539 2021:1–23. https://doi.org/10.1080/15583058.2021.1992539.

[9] Fortunato G, Funari MF, Lonetti P. Survey and seismic vulnerability assessment of the Baptistery of San Giovanni in Tumba (Italy). J Cult Herit 2017;26:64–78. https://doi.org/10.1016/j.culher.2017.01.010.

[10] Funari MF, Hajjat AE, Masciotta MG, Oliveira D v., Lourenço PB. A Parametric Scan-to-FEM Framework for the Digital Twin Generation of Historic Masonry Structures. Sustainability 2021, Vol 13, Page 11088 2021;13:11088. https://doi.org/10.3390/SU131911088.

[11] Katsanos EI, Sextos AG, Manolis GD. Selection of earthquake ground motion records: A state-of-the-art review from a structural engineering perspective. Soil Dynamics and Earthquake Engineering 2010;30. https://doi.org/10.1016/j.soildyn.2009.10.005.

[12] Araújo M, Macedo L, Marques M, Castro JM. Code-based record selection methods for seismic performance assessment of buildings. Earthq Eng Struct Dyn 2016;45. https://doi.org/10.1002/eqe.2620.

[13] Iervolino I, Maddaloni G, Cosenza E. A note on selection of time-histories for seismic analysis of bridges in Eurocode 8. Journal of Earthquake Engineering 2009;13. https://doi.org/10.1080/13632460902792428.

[14] Ugurhan B, Askan A. Stochastic strong ground motion simulation of the 12 november 1999 Düzce (Turkey) earthquake using a dynamic Corner frequency approach. Bulletin of the Seismological Society of America 2010;100. https://doi.org/10.1785/0120090358.

[15] Motazedian D, Atkinson GM. Stochastic finite-fault modeling based on a dynamic corner frequency. Bulletin of the Seismological Society of America 2005;95. https://doi.org/10.1785/0120030207.

[16] Karimzadeh S, Lourenço PB. Stochastic Ground Motion Simulation of the 9th of July 1998 Faial Earthquake (Azores, North Atlantic). Authorea Preprints 2022.

[17] Galasso C, Zhong P, Zareian F, Iervolino I, Graves RW. Validation of ground-motion simulations for historical events using MDoF systems. Earthq Eng Struct Dyn 2013;42. https://doi.org/10.1002/eqe.2278.

[18] Bijelić N, Lin T, Deierlein GG. Validation of the SCEC Broadband Platform simulations for tall building risk assessments considering spectral shape and duration of the ground motion. Earthq Eng Struct Dyn 2018;47. https://doi.org/10.1002/eqe.3066.

[19] Tsioulou A, Taflanidis AA, Galasso C. Validation of stochastic ground motion model modification by comparison to seismic demand of recorded ground motions. Bulletin of Earthquake Engineering 2019;17:2871–98.

[20] Karimzadeh S, Askan A, Yakut A, Ameri G. Assessment of alternative simulation techniques in nonlinear time history analyses of multi-story frame buildings: A case study. Soil Dynamics and Earthquake Engineering 2017;98. https://doi.org/10.1016/j.soildyn.2017.04.004.

[21] Zhong K, Lin T, Deierlein GG, Graves RW, Silva F, Luco N. Tall building performance-based seismic design using SCEC broadband platform site-specific ground motion simulations. Earthq Eng Struct Dyn 2021;50. https://doi.org/10.1002/eqe.3364.
[22] Code P. Eurocode 8: Design of structures for earthquake resistance-part 1: general rules, seismic actions and rules for buildings. Brussels: European Committee for Standardization 2005.
[23] Engineers AS of C. Minimum design loads for buildings and other structures, American Society of Civil Engineers; 2013.
[24] Macedo L, Castro JM. SelEQ: An advanced ground motion record selection and scaling framework. Advances in Engineering Software 2017;114. https://doi.org/10.1016/j.advengsoft.2017.05.005.
[25] Storn R, Price K. Differential Evolution - A Simple and Efficient Heuristic for Global Optimization over Continuous Spaces. Journal of Global Optimization 1997. https://doi.org/10.1023/A:1008202821328.
[26] Işık E, Büyüksaraç A, Ekinci YL, Aydın MC, Harirchian E. The effect of site-specific design spectrum on earthquake-building parameters: A case study from the Marmara region (NW Turkey). Applied Sciences (Switzerland) 2020;10. https://doi.org/10.3390/app10207247.
[27] Akkar S, Sandıkkaya MA, Şenyurt M, Sisi AA, Ay B, Traversa P, et al. Reference database for seismic ground-motion in Europe (RESORCE). Bulletin of Earthquake Engineering 2014;12. https://doi.org/10.1007/s10518-013-9506-8.
[28] Disaster, Authority EM. Turkish National Strong Motion Network 1973. https://doi.org/10.7914/SN/TK.
[29] Du W, Ning CL, Wang G. The effect of amplitude scaling limits on conditional spectrum-based ground motion selection. Earthq Eng Struct Dyn 2019;48. https://doi.org/10.1002/eqe.3173.
[30] Zengin E, Cakti E. Ground motion simulations for the 23 October 2011 Van, Eastern Turkey earthquake using stochastic finite fault approach. Bulletin of Earthquake Engineering 2014;12. https://doi.org/10.1007/s10518-013-9527-3.
[31] Karimzadeh S. Seismological and engineering demand misfits for evaluating simulated ground motion records. Applied Sciences (Switzerland) 2019;9. https://doi.org/10.3390/app9214497.
[32] Can G, Askan A, Karimzadeh S. An assessment of the 3 February 2002 Cay (Turkey) earthquake (Mw=6.6): Modeling of ground motions and felt intensity distribution. Soil Dynamics and Earthquake Engineering 2021;150. https://doi.org/10.1016/j.soildyn.2021.106832.
[33] Uckan E, Umut Ö, Sisman FN, c S, Askan A. Seismic response of base isolated liquid storage tanks to real and simulated near fault pulse type ground motions. Soil Dynamics and Earthquake Engineering 2018;112. https://doi.org/10.1016/j.soildyn.2018.04.030.
[34] Lulić L, Ožić K, Kišiček T, Hafner I, Stepinac M. Post-Earthquake Damage Assessment—Case Study of the Educational Building after the Zagreb Earthquake. Sustainability 2021, Vol 13, Page 6353 2021;13:6353. https://doi.org/10.3390/SU13116353.
[35] Lubliner J, Oliver J, Oller S, Oñate E. A plastic-damage model for concrete. Int J Solids Struct 1989;25:299–326. https://doi.org/10.1016/0020-7683(89)90050-4.